Density of States and Energy Gap in Andreev Billiards

A. Lodder

Faculteit Natuurkunde en Sterrenkunde, Vrije Universiteit, De Boelelaan 1081,
1081 HV Amsterdam, The Netherlands

Yu. V. Nazarov

Faculteit der Technische Natuurkunde and DIMES, Technische Universiteit Delft, Lorentzweg 1, 2628 CJ Delft, The
Netherlands
(February 1, 2008)

We present numerical results for the local density of states in semiclassical Andreev billiards. We show that the energy gap near the Fermi energy develops in a chaotic billiard. Using the same method no gap is found in similar square and circular billiards.

I. INTRODUCTION

The density of states in a normal metal in contact with a superconductor is affected by the superconductor, as a manifestation of the proximity effect or Andreev reflection. In early days of superconductivity, this effect has been observed in thin films of normal metal on a superconducting substrate.[1] It has been shown theoretically that for clean films the spectrum of quasiparticle excitations remains gapless[2] at Fermi energy, whereas a minigap develops for dirty films.[3] The energy scale of this minigap is given by $\hbar/t_N$, t_N being a typical time spent by an electron in the normal metal before it gets to the superconductor.[3]

Recent technological advances make it possible to study the effect in more complicated geometries, in diffusive metallic wires[4] and in a two-dimensional electron gas where electron transport is almost ballistic[5]. Recent theoretical developments[6,7] suggested a new interpretation of old results.[2,3] The existence of a minigap has been related to *chaotic* character of the electron motion in the normal part of the system. It makes no qualitative difference whether the electron transport is diffusive, as in dirty films, or chaotically ballistic, as in clean billiards[8]. The absence of the gap in the deGennes spectrum follows from the fact that a clean film is a specific case of a system with a separable geometry. In such a system the motion is not chaotic.

This interpretation is rather difficult to comprehend in semiclassical terms. That was the motivation of the present research. The problem is as follows. The electron motion becomes truly chaotic (ergodic) only for trajectories that are very long in comparison with the system size. As we show in detail below, long electron trajectories correspond to Andreev levels with energies very close to Fermi energy. Therefore, in contrast to the interpretation in question, one may argue that the presence of a minigap shows that there are *no* long trajectories in the system. Consequently, it may not be chaotic.
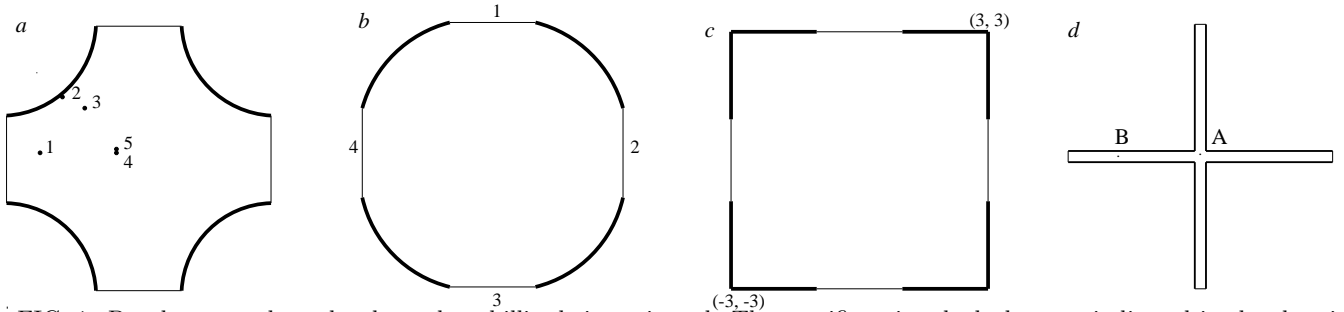

FIG. 1. Panels *a* to *c* show the three clean billiards investigated. The specific points looked at are indicated in the chaotic billiard. The four normal/superconducting interfaces are labeled in the circular billiard. Panel *d* shows the form of a quasi 1D diffusive system investigated as well.

To resolve this sophistry, we have calculated the density of states for several Andreev billiards, chaotic and non-chaotic, depicted in Fig. 1a to c. Such billiards combine Andreev[9] and specular reflection boundaries.[8] FIG. 1a shows the form of the chaotic billiard investigated. At the circular parts of the boundary specular reflection occurs, while at the straight linear parts Andreev reflection takes place. The outward concave shape of the circular parts make the system highly chaotic. The special form chosen can be considered as representative for any chaotic Andreev billiard.

arXiv:cond-mat/9801310v1 29 Jan 1998

In order to show the marked difference with related integrable Andreev billiards, calculations are done also for circular and square boundaries. These systems are depicted schematically in FIG. 1b and c. The three systems differ only as far as the specularly reflecting boundaries are concerned. Their Andreev reflecting boundaries are identical. FIG. 1d shows the form of a quasi one-dimensional diffusive system investigated as well.

To find the density of Andreev states, we solve the equations for the quasiclassical Green's function along each classical trajectory. The solution depends explicitly on the length L of the trajectory considered, and gives a set of energy eigenvalues $\simeq \hbar v_F / L$. Then, for each given point, we calculate numerically all possible classical trajectories and sum up their contributions to the density of states.

To put our results shortly, for the chaotic system we do observe the formation of a minigap near the Fermi level. Long, truly chaotic trajectories appear to take an exponentially small fraction of the phase volume and therefore do not contribute to the resulting density of states. The relevant equations are given in section II. Results are discussed in section III. Conclusions are formulated in section IV.

II. THE EQUATION FOR LOCAL DENSITY OF STATES

An expression for the local density of states $n(\epsilon, \mathbf{r})$ in the clean, ballistic systems to be considered, will be derived by taking the imaginary part of the local Green's function $G(\epsilon + i\delta, \mathbf{v}, \mathbf{r})$. The quasiclassical Green's function $G(i\omega_\mathrm{n}, \mathbf{v}, \mathbf{r})$ to be used will be a solution of the matrix equation[10,11]

$$\mathbf{v} \cdot \nabla G + i[H, G] = 0. \tag{1}$$

The velocity $\mathbf{v}$ is taken at the Fermi surface, the matrix H is given by

$$H = \begin{bmatrix} i\omega_\mathrm{n} & \Delta(\mathbf{r}) \\ -\Delta^*(\mathbf{r}) & -i\omega_\mathrm{n} \end{bmatrix}, \tag{2}$$

ω_n are the Matsubara frequencies and $\Delta(\mathbf{r})$ is the superconducting gap function, to be taken constant in the superconducting regions and zero in the central normal part of the system. Eq. (1) can be solved analytically for any trajectory. By accounting for all trajectories going through a given point the complete local solution can be found. We will show this by first writing Eq. (1) in the following from

$$v_\mathrm{F} \frac{\partial}{\partial \ell} G + i[H, G] = 0, \tag{3}$$

by which the $\mathbf{r}$ dependence is represented by the length parameter ℓ along a trajectory.

Suppressing the v_F dependence, the general solution can be written in the form

$$G_S(i\omega_\mathrm{n}, \ell) = c_1 A_S + c_2 B_S e^{\frac{2\sqrt{\omega_\mathrm{n}^2 + |\Delta|^2}}{v_\mathrm{F}}\ell} + c_3 D_S e^{-\frac{2\sqrt{\omega_\mathrm{n}^2 + |\Delta|^2}}{v_\mathrm{F}}\ell}, \tag{4}$$

in which the matrices A_S and B_S are given by

$$A_S = \frac{-i}{\sqrt{\omega_\mathrm{n}^2 + |\Delta|^2}} \begin{bmatrix} i\omega_\mathrm{n} & \Delta \\ -\Delta^* & -i\omega_\mathrm{n} \end{bmatrix}, \tag{5}$$

and

$$B_S = \frac{1}{2(\sqrt{\omega_\mathrm{n}^2 + |\Delta|^2})} \begin{bmatrix} -i\Delta^* & \omega_\mathrm{n} + \sqrt{(\omega_\mathrm{n}^2 + |\Delta|^2)} \\ -\frac{\Delta^*}{\Delta}(\omega_\mathrm{n} - \sqrt{(\omega_\mathrm{n}^2 + |\Delta|^2)}) & i\Delta^* \end{bmatrix}, \tag{6}$$

while $D_S = B_S^\dagger$. This solution is most easily obtained in two steps. First Eq. (3) is solved for the normal system, taking $\Delta(\mathbf{r}) = 0$ in the matrix H. One finds

$$G_N(i\omega_\mathrm{n}, \ell) = c_4 A_N + c_5 B_N e^{\frac{2\omega_\mathrm{n}\ell}{v_\mathrm{F}}} + c_6 D_N e^{-\frac{2\omega_\mathrm{n}\ell}{v_\mathrm{F}}}, \tag{7}$$

with matrices

$$A_N = \begin{bmatrix} 1 & 0 \\ 0 & -1 \end{bmatrix}, \text{ and } B_N = \begin{bmatrix} 0 & 1 \\ 0 & 0 \end{bmatrix}, \tag{8}$$

2

while $D_N = B_N^\dagger$. Since Eq. (3) is a homogeneous equation, the solution (7) is complete apart from an overall constant, to be determined by the requirement, that the matrix A_N times that constant is the solution of the original equation for the Green's function of a bulk system, still having a delta function at the right hand side. This will merely lead to the proper normalization[10] of the expression for the density of states to be derived below.

In the second step the full matrix H is diagonalized by the unitary matrix

$$U = \frac{1}{\sqrt{2}} \begin{bmatrix} \sqrt{(1 + \frac{\omega_n}{\sqrt{(\omega_n^2 + |\Delta|^2)}})} & \frac{i\Delta}{|\Delta|}\sqrt{(1 - \frac{\omega_n}{\sqrt{(\omega_n^2 + |\Delta|^2)}})} \\ \frac{i|\Delta|}{\Delta}\sqrt{(1 - \frac{\omega_n}{\sqrt{(\omega_n^2 + |\Delta|^2)}})} & \sqrt{(1 + \frac{\omega_n}{\sqrt{(\omega_n^2 + |\Delta|^2)}})} \end{bmatrix}. \tag{9}$$

The correspondingly transformed Eq. (3) has the same form as the equation for the normal system, the decay length being replaced by $v_F/\sqrt{(\omega_n^2 + |\Delta|^2)}$. Consequently, the full solution Eq. (4) of Eq. (3) now can be obtained by the unitary transformation $UG_N U^\dagger$ of the matrix given by Eq. (7), and substituting the proper decay length.

The solution of Eq. (3) for a trajectory in inhomogeneous systems as depicted in FIG. 1 is obtained as follows. Consider an arbitrary trajectory, hitting some point at one of the superconducting/normal interfaces, at which point an Andreev reflection takes place, and follow the trajectory inside the normal region by accounting for all specular reflections at the boundaries, until it hits a superconducting/normal interface again. If the length parameter ℓ is taken 0 at the initial hitting point and equal to L at the second hit, L standing for the total length of the trajectory, the form of the solutions in the different regions is clear from the Eqs. (4) and (7). For $\ell \leq 0$ and $\ell \geq L$ the solution (4) is to be used, Since the dimensions of the superconducting regions are supposed to be large, behaving effectively as bulk superconductors, the coefficient of the matrix A_S can be taken to be equal to 1. Further, for $\ell < 0$ the coefficient c_3 has to be put 0, while for $\ell > L$ the B_S term blows up and the corresponding coefficient has to be put 0. The normal region is supposed to have mesoscopic dimensions, and the full solution $G_N(i\omega_n, \ell)$ has to be used. The equation (3) being a first order differential equation, the only requirement is continuity at the interfaces. By that one finds for c_4 the following expression

$$c_4 = \frac{\omega_n}{\sqrt{\omega_n^2 + |\Delta|^2}} + \frac{|\Delta|^2 \tanh \frac{\omega_n L}{v_F}}{\omega_n^2 + |\Delta|^2 + \omega_n \sqrt{(\omega_n^2 + |\Delta|^2)} \tanh \frac{\omega_n L}{v_F}}. \tag{10}$$

Now everything is ready for the local density of states in the normal region. First of all, since we are after studying the development of a gap just above the Fermi energy and of a width much smaller than $|\Delta|$, it is sufficient to focus on the coefficient c_4 in the limit $|\omega_n| \ll |\Delta|$, so on

$$c_4 = \tanh \frac{\omega_n L}{v_F}. \tag{11}$$

Secondly, only the left upper matrix element of $G_N(i\omega_n, \ell)$ is required for the density of states, so only the c_4 term in Eq. (7) contributes. After the substitution $i\omega_n \to \epsilon + i\delta$, one finds the contribution of a trajectory of length L through a chosen point, to the density of states at that point, to be proportional to

$$\lim_{\delta \to 0} \Im i \tanh \frac{(\epsilon + i\delta)L}{iv_F} = \lim_{\delta \to 0} \Im \tan \frac{(\epsilon + i\delta)L}{v_F} = \pi \sum_n \delta(\frac{\epsilon L}{v_F} - (n + \tfrac{1}{2})\pi), \tag{12}$$

in which the summation runs over integer n values. For a given point in the interior region of a 2D system all trajectories through that point have to be taken into account. This leads to the following expression for the dimensionless local density of states $\nu(\epsilon, \mathbf{r})$, defined by

$$\nu(\epsilon, \mathbf{r}) \equiv \frac{n(\epsilon, \mathbf{r})}{n_N} = \int_0^\pi d\phi \sum_n \delta(\frac{\epsilon L(\phi)}{v_F} - (n + \tfrac{1}{2})\pi), \tag{13}$$

in which n_N is the constant density of states of a 2D normal system, and ϕ is the slope angle of a trajectory with length $L(\phi)$. For presenting the results it is most convenient to shift to the dimensionless energy variable $\eta \equiv \epsilon L_{\text{system}}/v_F$, in which L_{system} stands for the length dimension of the system. By that, and denoting the relative density of states, now depending on the variable η, by the same symbol ν, we end up at the expression

$$\nu(\eta, \mathbf{r}) = \int_0^\pi d\phi \sum_n \delta(\eta \frac{L(\phi)}{L_{\text{system}}} - (n + \tfrac{1}{2})\pi). \tag{14}$$

Note that in this final expression the length of a trajectory is present in a relative way, and has become dimensionless as well.

III. RESULTS AND DISCUSSION

Because Eq. (14) contains the relative quantity $L(\phi)/L_{\text{system}}$ only, the physical size of the system does not enter. However, in actual calculations a choice has to be made. We have chosen L_{system} to be equal to 6. In all systems depicted in FIG. 1 the origin lies in the center of the billiard. The corners of the square billiard then lie at $(\pm 3, \pm 3)$. The length of the S/N interfaces is chosen to be equal to 2. The specific points *1* to *5* to be looked at have the coordinates *1* $= (-2.2, 0.1)$, *2* $= (-1.7, 1.4)$, *3* $= (-1.2, 1.1)$, *4* $= (-0.5, 0.1)$ and *5* $= (-0.5, 0.2)$.

In FIG. 2 the density of states is shown for point *1* in the three billiards under consideration, for a ϕ-grid with $d\phi = \pi/200$. For comparison the results according to finer grids are shown in FIG. 5. In this figure the scale along the vertical axis has been adapted, by which the high peaks are not displayed fully, but the average structure comes out more clearly. The peak heights have been given explicitly. For the chaotic billiard, both figures show a gap at the Fermi energy, which corresponds with $\eta = 0$. The missing states in FIG. 2 near $\eta = 0$ for the square billiard are apparently due to the grid, because no gap is seen if ten and hundred times finer meshes are used. The finer mesh leads to a histogram, which is hardly distinguishable from a $d\phi = \pi/2000$ picture. But because of security all other histograms to be displayed are obtained using a $d\phi = \pi/20000$ mesh. The density of states $\nu_{\text{square}}(\eta)$ is quite similar for the different points, and no particular features show up, so we further concentrate on the circular and chaotic billiards.

The gap for the circular billiard is certainly typical for the point chosen. This becomes clear if one realizes, that states near $\eta = 0$ are due to trajectories, which are long compared to the system size. For the circular billiard such long trajectories contribute only if the line through a chosen point and the center of the circle hits a normal, specularly reflecting boundary. This requirement is not fulfilled for point *1*. At the top of FIG. 3 a similar plot is given, but for point *2*, for which such trajectories certainly contribute. Now no gap is seen for the circular billiard. The gap for the chaotic billiard is manifestly present in the middle of this figure, for point *2*, and at the bottom, for point *3*. The gap in the histogram for the circular billiard depends critically on the precise location of the point. This is shown in FIG. 4, displaying results for the points *4* and *5*. While point *4* does not support long trajectories, point *5* does. For the latter point the gap is closed, although it lies very near to point *4*. We show the histogram for the chaotic billiard at one of these points only, because not much difference is seen for this latter system.

For the chaotic system the gap is present for all points. It appears to be an intrinsic property of this system. Long trajectories are rare, irrespective of the point considered. While for the square and circular billiards trajectories with over 2000 times the system size are easily found, for the chaotic billiard it is hard to find trajectories longer than 20 times the system size. This is illustrated by TABLE I. The data given are obtained as follows. First, for fifty points the longest trajectory was calculated, using for each point a ϕ grid of $d\phi = \pi/2000$. The longest of the 100000 trajectories considered this way was found for point (-1.2, 0.9) at the angle given in the first line of the table in column 1. In addition to its length of 71.8 its relative length is given. In the last three columns the number of specular reflections and the labels of the S/N interfaces of both ends of the trajectory, called exits, are given. The meaning of these labels is shown for the circular billiard, in the middle of FIG. 1. After that the angle was specified finer and finer, using 10 angle values on both sides of the angle considered. Progressively the angle giving longest of the 21 lengths calculated that way was picked out for further subdivision. At the end, at one angle a length of 19.08 times the system size was found, but then the borderline of our (double) precision was reached. The sensitivity to the initial condition is illustrated by the results on the 5th and 8th line from the bottom, because they hold for the same angle. This angle was generated in a slightly different way in the subsequent subdivision. We conclude that long trajectories are rare, although, theoretically they are supposed to exist. For example, comparing the trajectories illustrated by the third and fourth line, there must be an angle ϕ_0 in between, at which the shift occurs from the first exit to the second one. This critical angle would support an infinitely long trajectory.

To give some qualitative estimations, we consider the contribution of the trajectories nearing that critical angle ϕ_0. The length at $\phi \to \phi_0$ can be estimated as $L(\phi) \simeq -L_{\text{system}} \log_2(|\phi - \phi_0|)$. This estimation follows from the fact that each bounce between concave boundaries approximately doubles the deviation angle. Using the relation (14) we estimate $\nu \simeq 2^{-\frac{\pi}{2\eta}}$. This shows that the density of states is exponentially suppressed at small η. With our numerical method, having a finite grid $\delta\phi$, we can only access energies $\eta \geq -\log_2(\delta\phi)$. The states with smaller energies are not seen. The good convergence of our numerical data, even at relatively small η, proves that the gap develops rather quickly, giving rise to an abrupt change of the density of states.

It is interesting to note that quantummechanical effects can also be estimated in this way. Due to diffraction of the electron waves in a billiard geometry, the best angle resolution is limited by $\delta\phi_\hbar = 1/\sqrt{k_F L_{\text{system}}}$, k_F being the electron wave vector at Fermi energy. This implies that no Andreev states exists below the threshold energy $\eta \simeq 1/\log_2(k_F L_{\text{system}})$.

Although it is not the primary aim of the present paper, it is interesting to discuss the structure seen in the histograms. The peaks are certainly due to the fact, that special classes of trajectories contribute more than an

TABLE I. Illustration of the fact, that long trajectories are rare in the chaotic billiard. From top to bottom increasing lengths $L(\phi)$ are found for an increasingly precisely chosen angle ϕ. The data are for a point somewhat below point 3, with coordinates (-1.2, 0.9).

ϕ in radians	$L(\phi)$	$L(\phi)/L_{\text{system}}$	No. reflections	Exit1	Exit2
-0.92677083000000	71.8	11.96	19	1	3
-0.92677083600000	75.5	12.59	21	1	1
-0.92677083700000	92.4	15.40	25	1	1
-0.92677083800000	70.8	11.80	20	1	2
-0.92677083690000	82.5	13.76	23	1	4
-0.92677083700000	92.4	15.40	25	1	1
-0.92677083710000	77.3	12.88	21	1	4
-0.92677083700000	92.4	15.40	25	1	1
-0.92677083701000	96.5	16.09	27	1	1
-0.92677083702000	77.8	12.97	22	1	4
-0.92677083700000	92.4	15.40	25	1	1
-0.92677083700100	110.3	18.39	30	1	3
-0.92677083700200	84.2	14.04	24	1	1
-0.92677083700090	88.9	14.82	25	1	4
-0.92677083700100	107.2	17.86	30	1	4
-0.92677083700110	91.0	15.16	25	1	3
-0.92677083700096	98.0	16.33	27	1	4
-0.92677083700097	114.5	19.08	32	1	2
-0.92677083700098	94.2	15.69	26	1	2

average trajectory. Considering the $L(\phi)$ dependence of the local density of states expression (14), for a given point and in an arbitrary direction this function will contain a term linear in ϕ. But there are exceptions. The length $L(\phi)$ for trajectories through the points 1, 4 and 5 in FIG. 1 behaves quadratically in ϕ around $\phi = 0$, while for the latter two points in addition a quadratic behaviour in $\phi - \pi/2$ around $\phi = \pi/2$ holds. Then the argument of the delta function in Eq. (14) behaves quadratically in ϕ around $\phi = 0$, giving rise to a *square root singularity* in the density of states. This singularity produces a series of equidistant peaks in the histogram with peak energies counted by the integer n. At $\phi = 0$ the length $L(\phi)$ is equal to L_{system}, so the lowest peak, for $n = 0$, is expected to be seen at $\eta = \pi/2 = 1.57$. This peak is easily recognized in the FIGs. 2, 5 and 4. Another type of trajectory in a direction ϕ_0, around which $L(\phi)$ behaves quadratically in $\phi - \phi_0$, is, for example, the one through point 3 in FIG. 1 with $\phi_0 \approx \pi/4$, hitting the exits 1 and 4. Since the line from the origin to point 3 has a slope that is slightly smaller than -1, ϕ_0 is not equal to $\pi/4$. The corresponding $L(\phi_0) = 5.23$, leading to a peak at $\eta = 1.8$, which is clearly present in the lower panel of FIG 3. The corresponding peak for point 2 lies too much to the right to be seen, namely at $\eta = 2.3$. We just point to another class of trajectories giving rise to quadratic behaviour, namely, for example, the one through point 3 and perpendicular to any outward concave circle. The corresponding line connects point 3 and the center of the circle. Although $L(\phi)$ behaves quadratic as far as the contribution towards the circle is concerned only, possible linear contributions from the backward part of the trajectory will lead to a shift of the extreme ϕ_0. We calculated the corresponding lengths, and, just as an illustration, we mention the peaks for a few points. The trajectory through point 1 perpendicular to the circle centered at (3, 3) leads to a peak at 0.97, which is clearly seen in the lower panels of FIGs. 2 and 5. The trajectories through point 2 perpendicular to the circles centered at (3, 3) and (3, -3) lead to peaks at 0.97 and 0.49 in the middle panel of FIG. 3.

Finally we want to point at even another type of extremal trajectory, namely a trajectory through a point and touching a circle. Consider the trajectory through point 2, in upward direction touching the circle centered at (-3, 3). The length has a minimum value at the touching angle ϕ_0, but the ϕ dependence remains linear. Still an effect can be expected, because the coefficient of $\Delta\phi \equiv \phi - \phi_0$ for positive $\Delta\phi$ can be different from the coefficient for negative $\Delta\phi$. This leads to a *step* in the evaluation of the delta function in the expression for the local density of states, because $\delta(b\Delta\phi) = \delta(\Delta\phi)/|b|$. In analyzing the different touching trajectories for the different points in the chaotic billiard, not all possible steps are clearly recognized, and others correspond to values of η, which lie too high to be seen. We

just mention the trajectory through point *2* touching the circle around (3, 3), which is expected to give a step at $\eta = 0.77$, and the trajectory through point *3* touching the circle around (-3, -3), corresponding to a step at $\eta = 1.35$. Both steps can be recognized in the middle and lower panel respectively of FIG 3.

We conclude by comparing the results for some point in the clean 2D chaotic billiard depicted by FIG. 1*a* with the local density of states at a central point A and a point B closer to the S/N interface in the *dirty* 1D Andreev billiard depicted in FIG. 1*d*. The results for the dirty system are obtained by numerical integration of the Usadel equations.[12] The curves A and B in FIG. 6 show the dimensionless density of states for the two points in the dirty 1D system, while the histogram holds for point 2 of the clean system and reproduces the lower energy part of the middle panel of FIG. 3. Mind, that the scale of the gap energy E_g is different in the ballistic and diffusive case: for a ballistic system $E_g \simeq \hbar v_{\mathrm{F}}/L_{\mathrm{system}}$, whereas for a diffusive system it is strongly reduced, $E_g \simeq \hbar v_{\mathrm{F}}/\sqrt{l L_{\mathrm{system}}}$, l being the mean free path. In order to compare results, the curves and the histogram are rescaled to a common E_g.

Despite the gap occurs in both cases, it is seen that the behavior of the density of states is quite different for diffusive and ballistic cases. Consequently, this behavior is not universal and depends on details of the geometry and the scattering within the billiard. This fact strongly reduces the applicability of Random Matrix Theory methods, which are based on the assumption of universality of chaotic behavior. We note that the absence of universality can be understood from the fact that long and truly chaotic trajectories do not contribute to the density of states. Therefore it is determined by non-ergodic, non-universal trajectories.

IV. CONCLUSIONS AND PROSPECTS

Our results prove that a gap is formed in the density of states of a chaotic Andreev billiard even in the semiclassical limit. This is despite the fact that in the semiclassical limit Andreev states could have a very small energy being generated by very long trajectories. It turns out that the density of states of a chaotic billiard exhibits an abrupt drop at energies several times smaller than $v_{\mathrm{F}}/L_{\mathrm{system}}$. Below this energy, the density of states is exponentially suppressed. We believe that quantum mechanical effects will lead to complete exhausting of the density of states at energies below $v_{\mathrm{F}}/(L_{\mathrm{system}} \log(k_{\mathrm{F}} L_{\mathrm{system}}))$. Comparison of the density of states in the billiard and in the diffusive system clearly shows the absence of even approximate universality.

For comparison a square and a circular Andreev billiard have been considered. In the square system long trajectories are always present, and no gap develops. Interestingly, although in roughly 70% of the volume of the circular system no gap is visible in the local density of states, in the remaining part of the volume there is also a gap developing. This possibly can be explained by the fact that the billiard is not ideally circular and may be slightly chaotic.

All three billiards exhibit geometrically induced features in the density of states. Trajectories that traverse a billiard perpendicular to the superconducting boundaries, without reflection, generate a sequence of equidistant square root singularities. Trajectories that touch concave boundaries lead to steps in the density of states.

[1] T. Claeson and S. Gygax, Sol. St. Comm. **4**, 385 (1996).

[2] P. G. de Gennes and D. Saint-James, Phys. Letters **4**, 151 (1963).

[3] W. L. McMillan, Phys. Rev. **175**, 537 (1968).

[4] S. Gueron, H. Pothier, N. O. Bridge, D. Esteve, and M. H. Devoret, Phys. Rev. Lett. **77**, 3025 (1996).

[5] S. G. den Hartog, B. J. van Wees, Yu. V. Nazarov, T. M. Klapwijk and G. Borghs, Phys. Rev. Lett. **79**, 3250 (1997), and references therein.

[6] J. A. Melsen, P. W. Brouwer, K. M. Frahm and C. W. J. Beenakker, Europhys. Lett. **35**, 7 (1996).

[7] A. Altland and M. R. Zirnbauer, Phys. Rev. Lett. **76**, 3420 (1996).

[8] M. V. Berry, Eur. J. Phys. **2**, 91 (1981).

[9] I. Kosztin, D. L. Maslov, and P. M. Goldbart, Phys. Rev. Lett. **75**, 1735 (1995).

[10] G. Eilenberger, Z. Phys. **214**, 195 (1968).

[11] M. Ashida, S. Aoyama, J. Hara, and K. Nagai, Phys. Rev. B **40**, 8673 (1989).
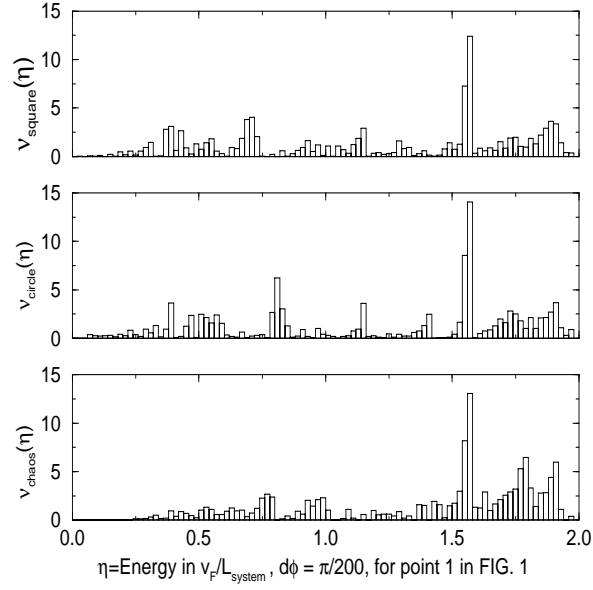
[12] K. D. Usadel, Phys. Rev. Lett. **25**, 507 (1970).

FIG. 2. From top to bottom the local density of states for the square, circular and chaotic billiards respectively, at point 1 in FIG. 1, for the ϕ-grid indicated along the horizontal axis.
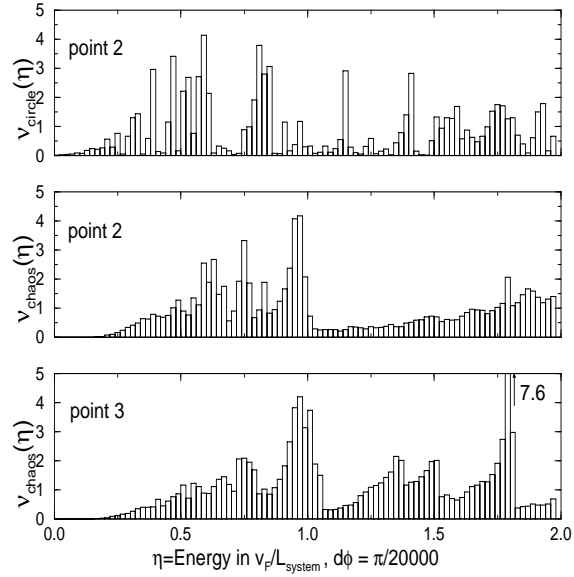

FIG. 3. The local density of states for the circular billiard at point 2, and for the chaotic billiard at the points 2 and 3 in FIG. 1.
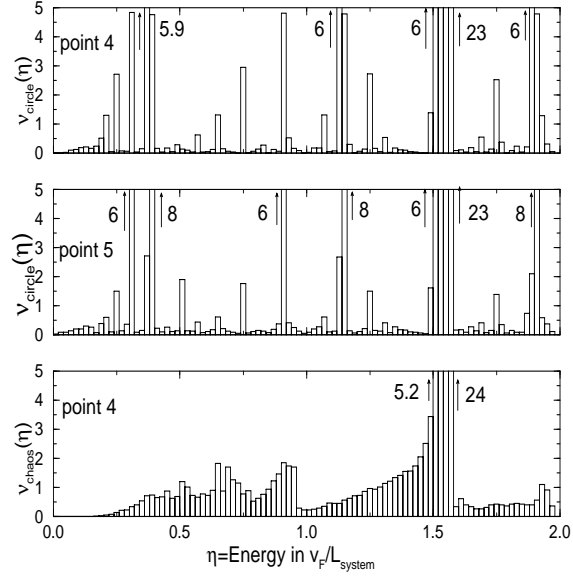
FIG. 4. The local density of states for the circular billiard at the points 4 and 5, and for the chaotic billiard at point 4.
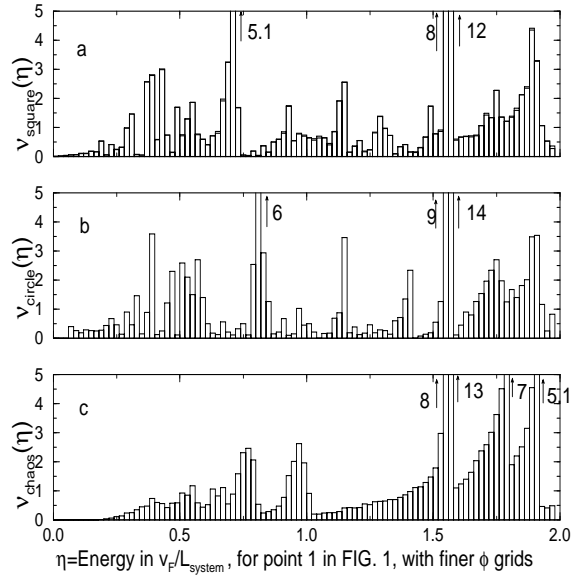

FIG. 5. The same as in FIG. 2, but for both a ten and hundred times finer ϕ-grid for the square billiard, and for a hundred times finer grid for the circular and chaotic billiards.
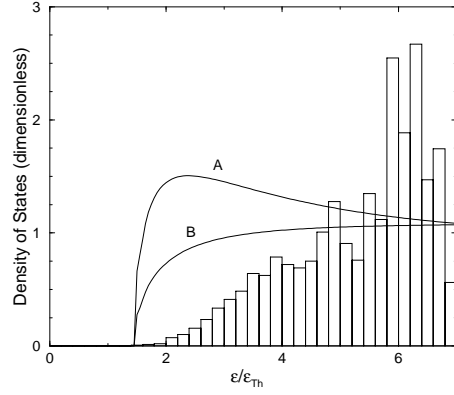
FIG. 6. The local density of states at the points A and B in the 1D dirty system depicted in FIG. 1d, compared with the histogram for point 2 in the 2D clean chaotic system depicted in FIG. 1a.